CERN Summer Studentship 2023
CMS iRPC assembly and Quality Control

Mohamed Gamal Ahmed Mohamed,
CERN, Geneva, Switzerland.

Supervisors:
Mehar Ali Shah
Mohammed Mahmoud Mohammed

Abstract

The CMS experiment at the LHC contributes significantly to understanding particle interactions. Among its detectors, RPC technology is vital for accurate muon identification and triggering. The introduction of iRPC enhances detector performance.

This summary introduces the importance of RPC detectors in CMS, highlighting their role in identifying muons, crucial for fundamental processes. RPC technology principles, like gas ionization and signal amplification, allow for precise time and space measurement.The report covers RPC evolution to iRPC, emphasizing improved materials and electronics. RPCs, with quick response and particle resistance, are integral to CMS's triggering.

The meticulous assembly of the CMS iRPC detector is summarized, involving careful component handling. The report explains procedures, including panel preparation, copper foil installation, and spacer positioning. Parallel steps for strip PCBs and bottom gap installation are outlined, followed by top gap alignment.

Contents

List of Figures

List of Tables

1 Introduction

1.1 The CMS Phase-2 upgrade

The CMS experiment, located at the LHC on the border of France and Switzerland, is a versatile venture that investigates proton-proton and heavy-ion collisions [10]. It has yielded significant insights into fundamental universal inquiries, notably co-discovering the Higgs boson with ATLAS in 2012 [1][2]. Operating at a record-breaking center-of-mass energy of up to 13.6 TeV and a luminosity surpassing 1034 $cm^{-2}s^{-1}$, the CMS has rigorously tested the Standard Model (SM) predictions with remarkable precision within an unparalleled energy spectrum.
Despite the fruitful contributions of the CMS Collaboration, the search for theoretically anticipated Beyond the Standard Model (BSM) particles remains challenging. Addressing this, a major enhancement termed HL-LHC or phase-2 has been devised for LHC systems. Envisioned for HL-LHC operations is a fivefold surge in integrated luminosity compared to initial design values [3][4]. As this upgrade will substantially heighten collision rates by a factor of 5, a comprehensive analysis of the adaptability of CMS detectors, especially the muon systems, is imperative. Consequently, an extensive research and development initiative has been established to ensure the continued efficiency and excellence of CMS muon systems.
As implied by its name, the CMS muon systems hold significance in the experiment since muon presence in the outcome of proton-proton collisions commonly signifies intriguing physics. Notably, a distinct indication of Higgs boson presence is its decay into four muons. Furthermore, it's suspected that the decay of numerous exotic yet undiscovered particles will yield multiple muons [5][6]. The CMS muon system encompasses three gaseous detector types. For precise muon trajectory assessment in the central barrel region ($|\eta| < 1.2$), Drift Tubes (DT) are employed. The endcap region employs Cathode Strip Chambers (CSC) for the same purpose. Both barrel and endcap regions utilize RPCs to produce rapid signals upon muon traversal, activating DTs, CSCs, and the broader CMS experiment data acquisition system. [5][12]
A primary hurdle for the HL-LHC enhancement revolves around reliable triggering of muon systems in the very forward regions. This domain poses challenges for muon detection due to the prevalence of high-pseudorapidity-produced light particles, such as muons. Concurrently, substantial backgrounds in the forward region necessitate intricate analysis. To augment the muon systems' detection capacity in this realm, novel muon detectors—GE1/1, GE2/1, RE3/1, and RE4/1 stations—will be integrated, spanning up to a pseudorapidity of 2.4. These additions furnish additional high-resolution measurement points, enhancing track reconstruction. In the existing muon stations YE1/1 and YE2/1, two fresh GEM detectors named GE1/1 and GE2/1 will be introduced. The vacant muon stations, YE3/1 and YE4/1 will be equipped with an enhanced version of RPC detectors termed RE3/1 and RE4/1. Given the projected HL-LHC rates, the current RPC detectors in this location will be inadequate, hence the development of the new iRPC detector [3].

1.1.1 CMS Resistive Plate Chamber (RPC)

The existing CMS experiment incorporates a total of 1056 RPC chambers. Among these, 480 chambers are situated in the barrel section, while the remaining 576 chambers are positioned in the endcap regions.[11] These chambers are systematically arranged into four stations named RB1 to RB4 in the barrel zone, and RE1 to RE4 in the endcap domain. The innermost stations in the barrel, RB1 and RB2, are outfitted with a pair of RPC chambers each, whereas all other RPC stations are equipped with a single RPC chamber. The complete RPC configuration is illustrated in figure 1.

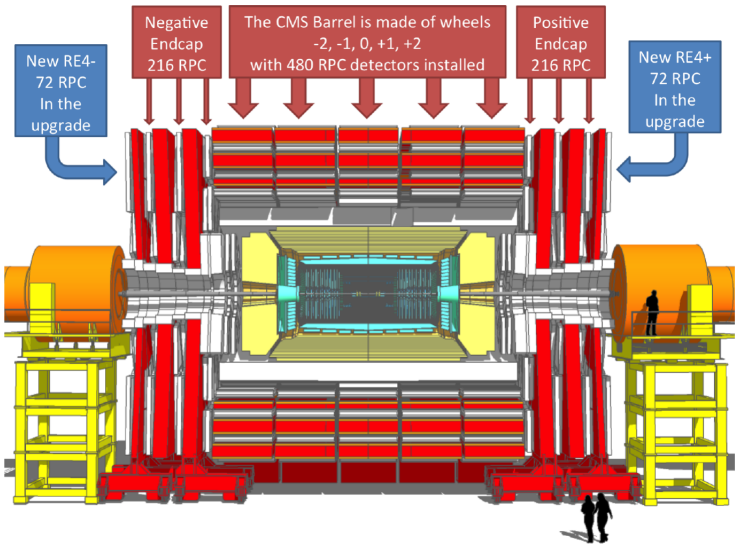

Figure 1: RPC chamber distribution in the Experiment.[5]

The CMS RPCs function as gaseous detectors featuring commendable time resolution (1 ns) and spatial resolution along the x axis ($\leq 10mm$). Their capability lies in detecting the traversal of charged particles[5]. These detectors consist of a dual-gap setup, where each gap comprises two electrode plates made of resistive High-Pressure Laminate (HPL), each with a thickness of 2 mm, and separated by a 2 mm gas layer. The external surface of the HPL plates is coated with a slender coat of graphite to which the high voltage is administered. The readout plane is constructed using copper strips on a mylar foil, positioned centrally between the two gas gaps. Operating in avalanche mode, the RPCs employ a gas mixture composed of95.2% freon ($C_2H_2F_4$), 4.5% isobutane (i–C_4H_{10}), and 0.3%sulfur hexafluoride (SF_6), while maintaining a relative humidity of $40-50\%$. The signals arising from the strips are transmitted asynchronously to the Front-End Board (FEB) housed within the chambers. Within the FEB, these signals are amplified, discriminated, and shaped [3][9].

1.1.2 Improved Resistive Plate Chambers (iRPC)

The pseudorapidity range characterized by high values presents notable challenges concerning muon triggering, identification, and measurement across various hadron colliders. The operational conditions foreseen during the HL-LHC phase, with expected elevated background and pile-up levels, will introduce difficulties in accurately identifying muons and correctly assigning their momentum (p_T) using the existing RPC detectors. Given these circumstances, enhancing the current RPC system and introducing new iRPC detectors in this specific region are imperative to maintain smooth operations during the HL-LHC era.
One of the key enhancements is to extend the coverage of the RPC in CMS from $|\eta| = 1.9$ to $|\eta| = 2.4$.[12] Enlarging this coverage range will lead to heightened efficiency in both trigger operations and offline reconstruction within a region characterized by substantial background and a relatively weak magnetic field within the muon system. Figure 2 depicts both the targeted region for the new iRPC systems' installation and the region of interest for the link system.

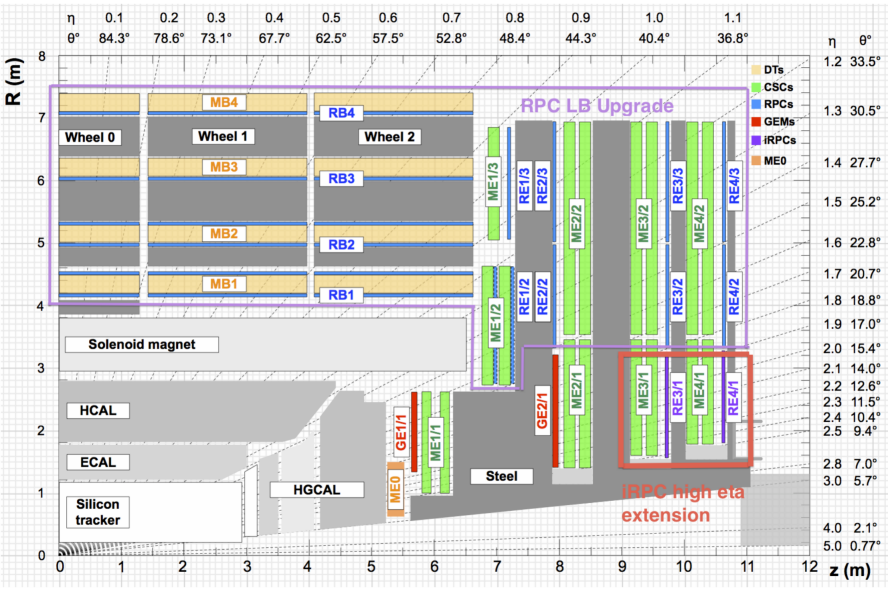

Figure 2: Quadrant of the CMS experiment.The red box indicates the region where additional RPCs will be placed to extend the muon coverage. The purple contour indicates the region affected by the link system upgrade.[3]

The upgraded iRPC system is anticipated to exhibit superior performance and durability in muon triggering, thereby achieving enhanced coverage within the extended η range. This coverage will align with that of the inner tracker and enable a novel independent trigger that incorporates inputs from both the tracker and RPCs. This advancement results from the combination of an improved gas detector version with new front-end electronics integrated with a high-precision timing mechanism. These enhancements facilitate more accurate determination of hits along the strip, alongside improved absolute time resolution and detector rate capabilities when compared to the existing RPC system. Consequently, the improved time resolution attained will open avenues for exploring various new physics channels involving long-lived particles, substantially bolstering the detection capabilities of the CMS muon system.
For the installation within the RE3/1 station, the iRPC will be affixed to the Endcap yoke 3 (YE3) iron disk, allowing it to cover the circular neutron shielding connected to YE3 and the cylindrical neutron shielding between yokes YE2 and YE3. Due to expanded $|\eta|$ coverage and space constraints, Front-End Boards (FEBs) will be positioned behind the iRPC chambers, necessitating chamber removal for access [7][8]. In the RE4/1 station, the iRPC chambers will be placed above the ME4/1 chambers in the high $|\eta|$ region, secured to an aluminum mounting frame attached to the rear of the CSC detectors [8].

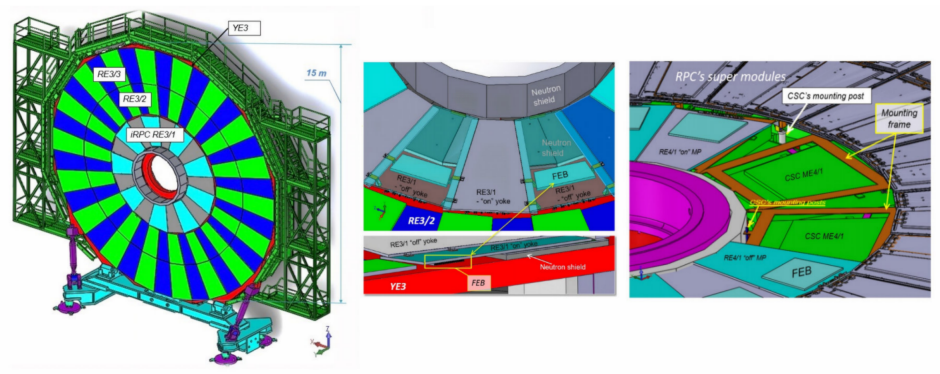

Figure 3: Detailed scheme of installation of the RE3/1 chambers on the YE3. 3D drawing of the RE3/1 chambers fixed on the YE3 (left). The FEBs mounted behind RE3/1 chambers (middle). Schematic view of the RE4/1 chambers mounted on the mounting plate (right). [8]

1.1.3 Improved RPC (iRPC) working principle.

A depiction of the iRPC chamber's layout can be observed in figure 1.3. Constructed as a dual-gap detector, the iRPC chamber comprises two 1.4 mm HPL electrodes forming each gap, with a gas gap of matching thickness in between. A distinct Front-End Board (FEB) was designed to read out both ends of pickup strips located on a Printed Circuit Board (PCB) panel positioned between these gaps. These gaps and PCB strips are safeguarded against electromagnetic interference by a copper layer, all encased within an aluminum (honeycomb) framework[7].

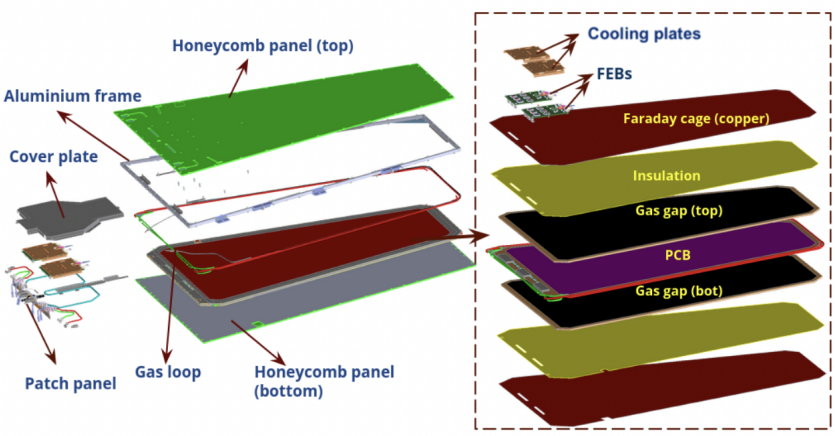

Figure 4: Schematic layout of the iRPC chamber.[8]

Each individual iRPC consists of a pair of HPL panels coated with a layer of graphite. Between these two panels, a spacer is inserted to determine the size of the gap. To establish the necessary electric field within the gap, the graphite coating of the panels is subjected to a high voltage.
The majority of gaseous detectors, including the iRPCs, employ the ionization process, wherein the passage of a charged particle through the chamber generates electron-ion pairs within the gas volume. Due to the external electric field, these electrons are propelled, causing further ionization and signal amplification. This results in a charge being induced on the anode located on the receiving strips, leading to a detectable signal by the FEB.

The decision was made to operate the iRPC in avalanche mode. In this operational mode, the ionization of gas by a passing charged particle generates a small number of electron-ion pairs in the gap. These pairs are subsequently accelerated by the electric field. The relatively high speed of electrons, owing to their lower mass, causes them to ionize additional gas molecules, triggering an avalanche of electrons moving toward the anode. This process generates an exceedingly swift signal, on the order of nanoseconds, which the front-end electronics can record[7].

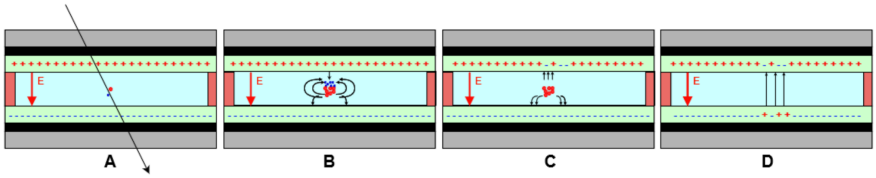

Figure 5: Schematic view of an iRPC operating in avalanche mode. (A) The passage of a particle ionizes molecules in the gas. (B) The size of the avalanche influences the local field. (C) The electrons reach the anode. (D) The ions reach the cathode. The charge is induced.[7]

The resulting signal is then analyzed using the Time Difference of Arrival (TDoA) technique. This method employs signals from both the High Radius (HR) and Low Radius (LR) sides of the detector, utilizing the time difference between their arrivals to pinpoint the signal's position along the strip. A schematic representation of this operational principle is depicted in figure 6.

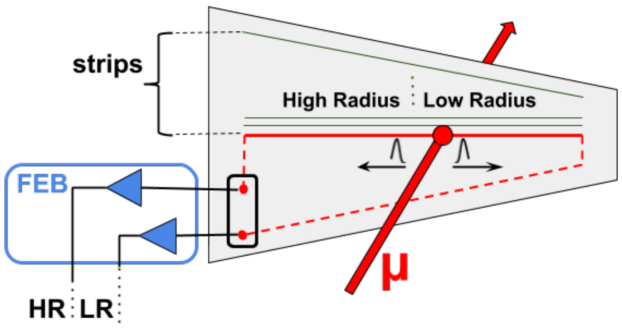

Figure 6: Schematic view of the working principle of an iRPC chamber with the TDoA method for calculating the position of the signal on the board.[7]

The TDoA method uses the information about the difference of arrival time from both ends of the pickup strip in order to estimate the position along a strip (Y), as follows,

$$Y = \frac{L}{2} - \frac{v.(t_2 - t_1)}{2}$$

From this it follows that the resolution of the position of a signal along the strip, using the TDoA method, is only limited by the electronics system and to a lesser extend by the resolution of the detector[7].
Based on this approach, a new specialised FEB was designed so as to provide two different arrival times (t_1 and t_2) corresponding to the arrival time of the signal to the two ends of the strip. Their difference can subsequently be used to determine the position of the signal along the strip following

the method described above. Using the signal speed propagation, one can use the sum of the two times to check that this corresponds to the strip's total length[7].

1.1.4 Difference between Resistive Plate Chamber (RPC) and improved RPC (iRPC)

In order to maximize the utilization of space within the inner layer endcap regions, the design of the new iRPCs was intentionally modeled closely after the existing wedge-shaped RPC detectors. The primary distinction in the chamber's design involves the utilization of thinner plates, which serves to decrease both the plate thickness and the gas gap from 2mm to 1.4mm. This adjustment yields several benefits; the reduction in electrode thickness and gas gap width leads to quicker recovery times for the electrodes and lowers the total charge generated during ionization avalanches. Moreover, curtailing the integrated deposited charge helps mitigate the aging process of the chamber. Nevertheless, the adoption of a slimmer chamber does result in a diminished gas gain for the recorded signal. To counterbalance this effect in the new iRPC chambers, a greater signal amplification is introduced through the new front-end electronics, accompanied by operation at a lower high voltage. An overview detailing the contrasts between the present RPC chambers and the novel iRPC detectors can be found in table 1.

	iRPC	RPC
High Pressure Laminate thickness	1.4 mm	2 mm
Num. of Gas Gap	2	2
Gas Gap thickness	1.4mm	2 mm
Resistivity (Ωcm)	$0.9-3x10^{10}$	$1-6x10^{10}$
Charge threshold	< 50 fC	150 fC
space resolution (eta)	1.5 cm	20-28 cm
space resolution (phi) strip pitch driven	0.3-0.6 cm	0.8-1.9 cm
Intrinsic time resolution	0.5 ns	1.5 ns

Table 1: Comparison between existing RPC and new iRPC chambers[8].

2 Assembly Procedures

The assembly procedures for the mechanical box assembly and iRPC chamber assembly involve a series of precise steps to ensure the proper construction of the assembly.
To begin with the Mechanical Box Assembly, the process starts by placing the bottom honeycomb panel on a table with the inner surface facing up. Protective film is removed from the inner surface, and thorough cleaning is done on all sides, including the HV cut hole. Kapton tape is applied over the HV cut hole. The next step involves selecting and cleaning the appropriate side bars and positioning them over the bottom panel. L-shape spacers are inserted and secured with screws to fix the side bars in place. Afterward, the bottom panel is turned, and the protective film is removed.

Moving on to the Top Panel Preparation, the top honeycomb panel is readied with M3 nuts, and M8 holes are cleaned. Tools for M3 nuts are inserted, glue is applied to the holes, and excess glue is removed, allowing the panel to harden. The Top Panel Closure Preparation involves cleaning edges and holes, removing protective film, and applying Kapton tape to the HV pad.
Now, shifting to the iRPC Chamber Assembly Procedure, it begins with placing the prepared bottom panel onto the assembly table, complete with L-shape spacers and side bars. Vacuum aspiration is used to clean the inner area of the box, and the inner box surface is further cleaned with alcohol. The bottom copper foil is prepared by cleaning it and soldering copper strips along the edges. This copper foil is then installed. L-shape spacers are adjusted outward, and the bottom mylar is placed on the copper foil. The HV pad is cleaned once more.
Simultaneously, the strip PCB is prepared by cleaning both surfaces and securing them together with Kapton tape while maintaining a precise spacing. The bottom gap is also prepared, with Teflon protection added to the HV pad. The gap is installed inside the chamber, and L-shape spacers are adjusted to align with the side bars.

Gas pipes for the bottom gap are installed, and the gap is secured in place with screws and plastic filler. Protective film is removed from the ground side of the bottom gap. The strip PCB plane is installed, and the top gap is prepared, flipped into the chamber, and centered between L-shape spacers. Gas pipes for the top gap are prepared similarly to the bottom gap. Protective film is removed from the ground side of the top gap, and extra Teflon protection is added.




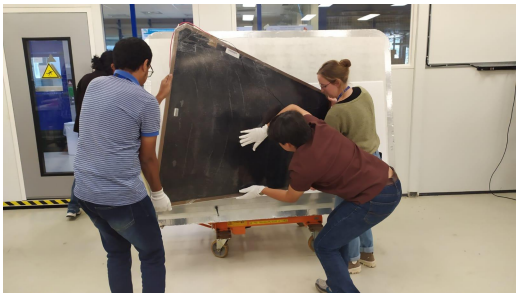

The top copper foil is prepared, including creating holes and soldering grounding foils in place. The top mylar is installed, cut around the HV pad, and preparations for the chamber FOS are made. The chamber is prepared for closing with copper tape, T-connectors, and support for plastic pipes. Gas unions are ensured to be tightly connected. The top honeycomb panel is placed over the Faraday cage, and the chamber is closed. FEB grounding foils are taped to the outer top honeycomb panel surface. The patch panel and copper grounding bar are installed, and copper gas pipes are connected to chamber openings on the top panel. Finally, the FOS LC connector is prepared and installed on the patch panel.


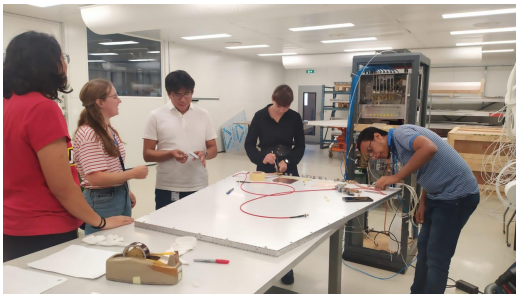

3 Quality Control tests

The objective of this test is to investigate the behavior of the detector in actual LHC conditions. It aims to confirm the functionality of the iRPC FEB and backend electronics, as well as the integration of the new RPC stations into the CMS Detector Control Software and Data Acquisition system. The protocols for Quality Control (QC) have been established and documented since 2010. The QC process for gap level assessment includes multiple steps. These involve visually inspecting the gaps, confirming spacer conditions, ensuring gas tightness, and conducting dark current tests.

Figure 1 illustrates the results of the QC tests performed on a gap. In the first graph, pressure data from the gas leak test is presented, with a blue line indicating the actual data. The calculated pressure drop is 0.028 mbar/10 min, which is within the acceptable limit of 0.4 mbar/10 min.
The second graph displays pressure data from the spacer test. The blue line corresponds to the collected data. Each spike on the graph corresponds to a spacer within the gap, and the smooth transitions suggest good spacer conditions.
The third graph depicts the variation of dark current concerning the applied HV. Following the assembly, the chamber undergoes visual inspections of mechanics, gas leak tests, and dark current tests as part of the chamber-level QC. These assessments are conducted at CERN's building 904.[13]

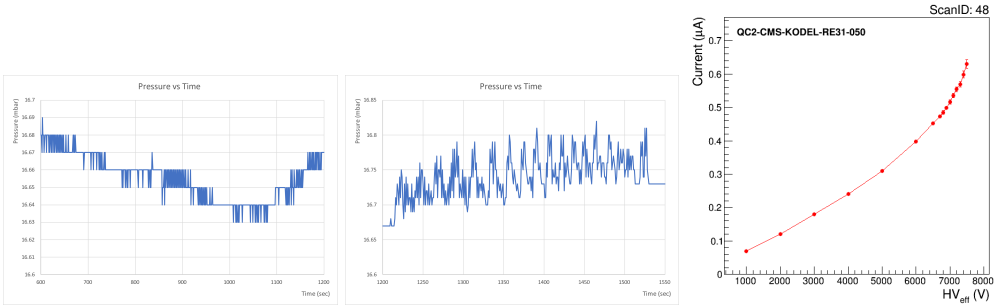

Figure 7: Results of gap level QC performed at a laboratory: Leak test (left), Spacer test (middle), Dark current test (right)

A longer test with cosmic rays will be performed to monitor the chamber performance at different high voltages (HV). To test the detectors, we have a cosmic setup in Building 904 that uses cosmic rays to study the effects on the chamber.
The cosmic setup includes the chamber and two scintillators, one at the top and one at the bottom. These scintillators allow us to confirm that a particle has passed through the chamber by detecting a coincidence event, which occurs when an event is detected in both scintillators. We used RE3/1-197 to collect data for this test, which took about 16 hours.

The efficiency is estimated as the ratio of the number of detected muons to the total number

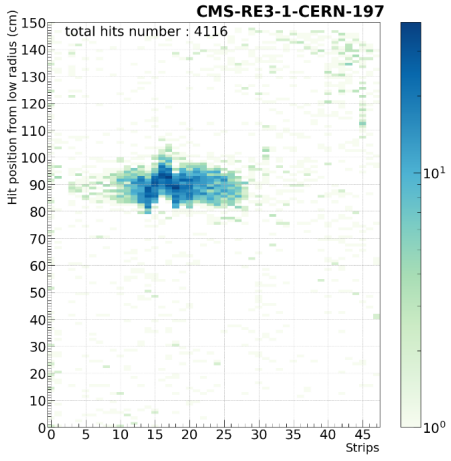

Figure 8: Hit map of the event detected by the half chamber.

of triggers. The signal arrival time of each of the two ends of the strip must be within a time

window associated with the external trigger. This time window depends on the area covered by the scintillators along the strips. We can determine the width of this window by the blue and green spots in the hit map of Figure 8, which shows the part of the chamber that detected the events. Once we have determined the window, we can plot the efficiency as a function of the HV, as shown in Figure 9 for the chamber test.
One of the important parameters that we can determine from the efficiency plot is the working point (WP). To determine the optimal WP for each prototype, we study their efficiency as a function of the applied effective HV. Therefore, HV scans are performed. The goal of the HV scan is to study the efficiency as a function of the HV for all the iRPC prototypes to find the best working HV for each chamber, as well as to study the cluster size associated with the passage of a muon and to estimate the noise rate.

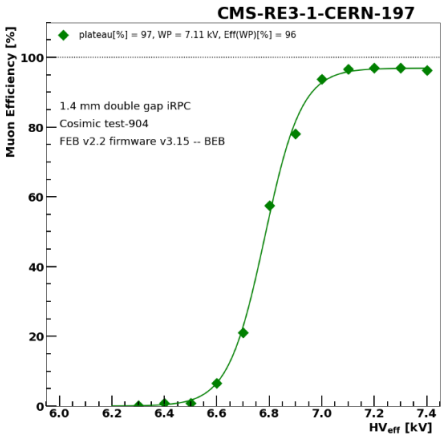

Figure 9: Example of a high voltage scan. The green triangles correspond to the calculated efficiency at the given HV points. The green curve gives the fitted sigmoid function to the efficiency as a function of the applied effective HV.

The efficiency curve is usually well described by a sigmoid function:

$$\epsilon = \frac{\epsilon_{max}}{1 + e^{-\lambda(HV_{eff} - HV_{50})}}$$

Where $\epsilon$is the efficiency at a given HV_{eff} , ϵ_{max} is the plateau of this fit function, It is determined by the slope of the fit function at HV_{eff} corresponding to 50 percent of the maximal efficiency. This can be expressed by the following formula:

$$slope = \frac{d\epsilon}{d(HV_{eff})} = \frac{\lambda\epsilon_{max}}{4}$$

To determine the working point, we use the following definition adopted by the CMS collaboration for the 2 mm gas gap RPC:

$$WP = HV(50) - \frac{loglog(\frac{1}{0.95} - 1)}{\lambda} + 150(V)$$

and the working point is determined in Figure 9 which is close to 7.11 kV.

4 conclusion

In the HL-LHC, the background rates in the RE3/1 and RE4/1 regions are expected to be 10 times higher than those we have experienced in the existing endcap RPCs. To maintain the robustness and redundancy as well as the identification and reconstruction capabilities of the muon system, the RPC upgrade project is presented. The thickness of the gas gap and of the RPC electrodes is chosen as 1.4 mm rather than 2 mm, which has been used for the existing RPC system. The choice of the thinner thickness is to ensure a shorter removal time of the avalanche charge through the RPC electrodes which enhances the rate capability. Also, use of a lower threshold permits to preserve the size of the operational plateau of the previous RPC version. The reduction of operational high voltage will reduce the risk of detector aging and helps to improve robustness of the high voltage system. It fulfills the requirements of operation in the high background rates of the HL-LHC phase: the efficiency at particle rates of 2 kHz/cm2 which is (a factor of 3 higher than the mean value expected in the iRPCs in future HL-LHC runs) is higher than 95%.[14]
This report emphasizes the role of iRPC detectors in CMS, contributing to muon identification and triggering. RPC and iRPC detectors remain essential tools as CMS advances particle physics. This encapsulates the complexities of assembling and testing the CMS iRPC detector, offering insights for integration.

References

[1] G. Aad et al.,*"Observation of a new particle in the search for the standard model higgs boson with the ATLAS detector at the LHC,"*, Physics Letters B, vol. 716, pp. 1–29, sep 2012.

[2] S. Chatrchyan et al., *"Observation of a new boson at a mass of* 125 *GeV with the CMS experiment at the LHC,"*, Physics Letters B, vol. 716, pp. 30–61, sep 2012.

[3] *"The Phase-*2 *Upgrade of the CMS Muon Detectors,"*, tech. rep., CERN, Geneva, Sep 2017. This is the final version, approved by the LHCC.

[4] "G. Apollinari et al., *"High-Luminosity Large Hadron Collider* (*HL-LHC*)*"*, Technical Design Report V. 0.1. CERN Yellow Reports: Monographs, Geneva: CERN, 2017.

[5] A. L. Cabrera Mora, *"CMS Resistive Plate Chambers performance at* $\sqrt{s}$ =13 *TeV,"*, tech. rep., CERN, Geneva, Dec 2016.

[6] A. L. Cabrera Mora, *"Status and performance of the CMS muon system in Run*2*,"*, tech. rep., CERN, Geneva, Oct 2016.

[7] K. Shchablo, *Development of fast timing detector for CMS experiment upgrade at CERN.*, Theses, Universit´e de Lyon, Dec. 2020.

[8] Voevodina, E. and others, *"RE*3*/*1 *RE*4*/*1 *RPC chambers integration in the inner region of the forward muon spectrometer in the CMS experiment,"*, JOURNAL OF INSTRUMENTATION, vol. 14, p. 6, 2019.

[9] K. Shchablo, *"Front-End electronics for CMS iRPC detectors,"*, tech. rep., CERN, Geneva, Apr 2020.

[10] CMS collaboration, *The CMS Experiment at the CERN LHC*, 2008 JINST 3 S08004.

[11] G. Pugliese [CMS Muon Collaboration], *The RPC system for the CMS experiment*, IEEE Nucl. Sci. Symp. Conf. Rec. 2 (2007) 822.

[12] CMS collaboration, *Performance of the CMS muon detector and muon reconstruction with proton-proton collisions at* ps= 13 *TeV*, 2018 JINST 13 P06015 [arXiv:1804.04528].

[13] A. Samalan and on behalf of the CMS Collaboration,*Improved Resistive Plate Chambers for the upgrade of the CMS muon detector*, J. Phys.: Conf. Ser. 2374 012006

[14] P. Kumari et al *Improved-RPC for the CMS muon system upgrade for the HL-LHC*,2020 JINST 15 C11012